Alexandria Engineering Journal (2023) 76, 19–33

HOSTED BY

Alexandria University

Alexandria Engineering Journal

www.elsevier.com/locate/aej
www.sciencedirect.com

ORIGINAL ARTICLE

Numerical simulation of convection hybrid ferrofluid with magnetic dipole effect on an inclined stretching sheet

Nur Ilyana Kamis, Lim Yeou Jiann, Sharidan Shafie, Noraihan Afiqah Rawi *

Department of Mathematical Sciences, Faculty of Science, Universiti Teknologi Malaysia, 81310 Johor Bahru, Johor, Malaysia

Received 11 April 2023; revised 30 May 2023; accepted 9 June 2023
Available online 17 June 2023

KEYWORDS

Hybrid magnetic nanoparticles;
Magnetic dipole;
Inclined stretching sheet;
Keller box method

Abstract Iron oxide nanoparticles possess magnetic characteristics that enable their control and manipulation using external magnetic fields, making them suitable for a wide range of biomedical engineering applications. Consequently, this study investigates the ferrohydrodynamic interaction of hybrid magnetic nanoparticles in an ethylene glycol plus water mixture flowing over an inclined stretching sheet, taking into account the magnetic dipole effect. The governing partial differential equations are transformed into ordinary differential equations by opting the suitable similarity variables. To obtain the numerical results, an unconditionally stable implicit difference method called the Keller box method is employed. The study analyzes the effects of the inclination angle, ferrohydrodynamic interaction, ferroparticle volume fraction, and mixed convection parameter. The results indicate that an increase in the inclination angle and mixed convective parameter enhances the velocity profile and Nusselt number, whereas the ferrohydrodynamic interaction and ferroparticle volume fraction exhibit the opposite trend. Furthermore, the study reveals that under certain conditions, the presence of magnetic oxide and cobalt iron oxide suspended in an ethylene glycol plus water mixture effectively reduces the heat transfer rate.

1. Introduction

Magnetic fields are significant in regulating the movement of fluids and energy transfer in numerous industrial and technical procedures such as liquid cooling systems, nuclear reactors, and the refining of molten metal. Magnetohydrodynamics (MHD) and ferrohydrodynamics (FHD) effects result from the applied magnetic field induced by the Lorentz force [1] and Kelvin force, respectively [2]. The volume forces of MHD formulated the electrically conducting fluids while FHD involved the polarization and magnetization along with non-conducting electrical fluid [3]. Some fruitful articles on MHD flow have been presented in [4–10]. In order to process of generating the FHD effect, the magnetic material is required to form either magnetic lines or fields [11]. One of the most well-known magnetic materials in the industry is the magnetic dipole, which creates a magnetic field and so causes the fluid to

* Corresponding author.
E-mail address: noraihanafiqah@utm.my (N.A. Rawi).
Peer review under responsibility of Faculty of Engineering, Alexandria University.

https://doi.org/10.1016/j.aej.2023.06.030

Nomenclature

U_w	stretching velocity	d	distance of the magnetic dipole
T_w	sheet temperature	K	thermomagnetic
T_∞	ambient or bulk temperature	Pr	Prandtl number
T_c	Curie temperature	ε	Curie temperature
(u, v)	velocity components for (x, y)	χ	viscous dissipation
ρ	density	β	ferrohydrodynamic interaction parameter
μ	dynamic viscosity	α	dimensionless distance
ρC_p	heat capacity	λ	mixed convection
k	thermal conductivity	Gr_x	Grashof number
T	temperature	Re_x	Reynold number
M	magnetization	C_f	local skin friction
H	magnetic field	Nu_x	Nusselt number
g	gravitational acceleration	τ_w	wall shear stress
β^*	thermal expansion	q_w	heat transfer rate
α^*	inclination angle		

experience the FHD effect. The magnetic dipole is a microscopically small magnet including a bar magnet. Cullity and Graham [12] who explained the magnetic background claimed that the magnetic dipole is a relatively short magnet of the finite moment. In view of this fact that similar magnetic field exists even though the length of the magnetic bar is cut to its maximum limit and doubles its pole strength. In terms of its physical composition, a magnetic bar is composed of two poles - north and south. The strength of the magnetic field is determined by the product of the magnet's length and strength. Kira *et al*. [13] investigated magnetic dipole modeling and concluded that the smaller distance of the spherical magnetized dipole provides the nearest field line on the bar magnet, demonstrating a strong magnetic field.

According to an analytical solution on heat transfer with thermomagnetic and magneto-mechanical effects that have been reported by Neuringer and Rosensweig [14], the presence of ferrofluid in a magnetic field produces a helpful FHD effect for fluid flow owing to thermal energy exchange in the fluid. The iron oxide that dissolved in a nonmagnetic carrier fluid is called ferrofluids and was synthesized in 1960 [15]. Ferrofluids are stable industrially prepared magnetic fluids and consist of a highly colloidal suspension of magnetic particles with ten nanometers in diameter [16]. The liquid carrier is an electrically non-conducting fluid encompassed with polar and nonpolar fluid. Magnetic nanoparticles have excellent physical and chemical properties, including being stable, environmentally safe as well as biocompatible [17]. Therefore, it leads to significant research development in the field of medical and pharmaceutical industries specifically in cancer therapy (treatment for hyperthermia), drug delivery, and magnetic resonance imaging (MRI) [17,18].

Andersson and Valnes [19] first investigated the ferrofluid model under the influence of magnetic dipole along with a stretching sheet. A magnetic dipole is applied under the sheet in a positive x direction. The magnetic field intensity increases as the sheet is stretched, saturating the ferrofluid. Thus, it reduces the heat transfer rate at the sheet. The numerical results without ferrohydrodynamics interaction show good agreement with the analytical solution proposed by Crane [20]. Titus and Abraham [21] were inspired by the work done by [19] and then conducted a report on the pattern of ferrofluid flow over an inclined stretching sheet together with prescribed surface temperature (PST) and prescribed heat flux (PHF). The results show that an angular enlargement of the sheet when stretched increases the fluid velocity, however, reducing the temperature distribution for both the PST and PHF cases. The outcomes have been parallel with the numerical results obtained by Zeeshan *et al*. [22]. The effect of the Grashof number as the parameter of mixed convection controls the fluid flow under the magnetic dipole effect [22,23]. Punith Gowda *et al*. [24] reduced the complexity of the governing equations of ferrofluid [19] by applying the boundary layer approximation theorem.

Heat transfer of nanofluid exhibits superior thermophysical attributes than the conventional base fluid in terms of thermal conductivity, thermal diffusivity, viscosity, and convective heat transfer coefficient. The reason for this is that traditional heat transfer fluids have low thermal conductivity when compared to solids. As a result, scientists have attempted to create fluids that use uniformed dispersion and stable suspension of solid nanoparticles to improve the low thermal conductivity of these traditional heat transfer fluids. The combination of the metal oxides and ferromagnetic nanoparticles dispersed in a carrier fluid such as oil, water, or ethylene glycol are categorized as nano-ferrofluids [25]. This approach is consistent with the nanofluid hypothesis, which was initially proposed by Choi and Eastman [26] in 1995 s, and states that a nanofluid is a mixing of a tiny amount of nanoparticles and a base fluid. Hence, nano-ferrofluids ferrimagnetic materials are nanofluids due to the reaction of metal oxides containing nano-ferric ions $\left(Co^{2+}, Mn^{2+}, Zn^{2+}\right)$ into a magnetic material (ferrofluids) with the oxidation state + 2 metals [27]. Consequently, the physical and chemical properties of nano-ferrofluids also attract interest among the academic and industrial communities to explore the theoretical study of ferrimagnetic. The theoretical study of the magnetic dipole in nano-ferrofluids which is the nickel-zinc ferrite ($NiZnFe_2O_4$) and manganese zinc ferrite ($MnZnFe_2O_4$) with hematite ferrite (Fe_2O_4) in ethylene glycol [28,29] and water [29,30], magnetite (Fe_3O_4) in three base fluids such as kerosene, water, and refrigerant-134a [31], paramagnetic tantalum (Ta), diamagnetic copper (Cu), and ferromagnetic (Fe) which dissolved in base fluid 60% ethylene glycol and 40 % water [32] and Fe against Fe_3O_4 in ethylene glycol with water

[33]. Sheikholeslami [34] extended the work Sheikholeslami [35] by considering the MHD effect on Fe_3O_4 in water by using a new numerical approach, numerically.

The mixes of nanoparticles termed "hybrid nanofluids" have gained a response from various industries that are interested to explore it more deeply due to its extensive technical, industrial, and scientific applications such as for transportation, microfluidics, medical manufacturing and so on. Hybrid nanofluids are formed by the suspension of two different types of non-magnetic nanoparticles, whereas hybrid ferrofluid are manufactured by the mixing of double magnetic nanoparticles in conventional liquids. Kiranakumar, Thejas [36] claimed that hybrid materials have high sensitivity and are more suitable for room-temperature operation than single fluid. A comparison theoretical study of hybrid ferrofluid and hybrid nanofluids with magnetic dipole that has been reported by Naveen Kumar *et al.* [37] proved that the hybrid ferrofluid $MnZnFe_2O_4 - NiZnFe_2O_4$ in ethylene glycol improved the minimum heat transfer together with velocity field contrast to hybrid nanofluids. However, the temperature field of hybrid nanofluids is higher than hybrid ferrofluid. In addition, hybrid ferrofluid of $Fe_3O_4/CoFe_3O_4$ (magnetite and cobalt magnetite) in engine oil depict more positive effects against heat transfer rate [38]. When compared to hybrid nanofluids, the flow characteristics of hybrid ferrofluid are easier to regulate using electromagnetic induction. It is interesting to mention that the research on $Fe_3O_4/CoFe_3O_4$ by addressing the MHD effect has been reported by Ramesh *et al.* [39] and Zainodin *et al.* [40].

The mathematical formulation in the biomedical field has been done by several researchers [41–43]. Therefore, the present study will analyze the magnetic nanoparticles in biomedical engineering applications namely MRI, and cancer treatment, where they can be implanted into tumor tissue and heated using an external magnetic field. The primary aim of this study is to explore the characteristics of magnetic nanoparticles. While many researchers have studied the magnetic dipole effect in fluid flow, there has been relatively little investigation into the behavior of a hybrid ferrofluid over an inclined stretching sheet. Therefore, the present study is inspired by the prior study of ferrofluids [19] to explore the behavior of hybrid ferrofluid. To achieve this, the problem is expanded from [24] to include an inclined stretching sheet [21]. Hybrid nanoparticles based on the previous study [38] and dissolved in a mixture of ethylene glycol and water [32,33], are chosen for the study. Using the similarity transformation technique, the governing partial differential equations (PDEs) are altered into ordinary differential equations (ODEs). To solve these ODEs, the Keller box method, which is an implicit difference framework known for its absolute stability, is employed.

2. Mathematical formulation

In this study, the mathematical formulation is addressed by following these conditions and assumptions:

- an incompressible and laminar steady fluid flow,
- two-dimensional Newtonian boundary layer flow,
- hybrid ferromagnetic fluid,
- boundary layer approximation,
- boussinesq approximation,
- magnetic dipole in terms of ferrohydromagnetic effect,
- inclined stretching sheet,
- no slip boundary conditions.

The mathematical model demonstrates the hybrid ferrofluid flow past an inclined stretching sheet. The sheet is stretched along the $x-$ axis with the velocity, $U_w = cx$ where c is a constant value, as well as y is perpendicular to the sheet at the $x-$ axis. As illustrated in Fig. 1 [44,45], the magnetic dipole is located below the sheet and the center lies on the $y-$ axis with some distance, d. The ferrofluid is confined to the half-space of positive y at the sheet. By generating a magnetic field that points in the x direction, the magnetic dipole strengthens the magnetic force and induces saturation in ferrofluids. Moreover, the sheet is set with a fixed temperature, T_w. The ambient fluid temperature or bulk fluid temperature as discussed by Das *et al.* [46] is taken to be T_∞. The temperature of the fluid far away from the surface of the sheet where the ferromagnetic element starts to lose its magnetism and become paramagnetic is given as the Curie temperature, T_c and $T_c = T_\infty$. The mixtures of two kinds of nanoparticles in ferrofluids and suspended in the base fluid produce hybrid ferrofluid. By applying a modification of the Tiwari and Das model [40] the governing equations including continuity, momentum, and energy equation can be written as [19,21,24]

$$\frac{\partial u}{\partial x} + \frac{\partial \upsilon}{\partial y} = 0, \tag{1}$$

$$\rho_{hnf}\left(v\frac{\partial u}{\partial y} + u\frac{\partial u}{\partial x}\right) = M\mu_0\frac{\partial H}{\partial x} + \mu_{hnf}\left(\frac{\partial^2 u}{\partial y^2} + \frac{\partial^2 u}{\partial x^2}\right) + g\beta^*(T_c - T)\ \sin\ \alpha^* \tag{2}$$

$$\left(\rho C_p\right)_{hnf}\left(v\frac{\partial T}{\partial y} + u\frac{\partial T}{\partial x}\right) + \left(v\frac{\partial H}{\partial y} + u\frac{\partial H}{\partial x}\right)\mu_0 T\frac{\partial M}{\partial T} = k_{hnf}\left(\frac{\partial^2 T}{\partial y^2} + \frac{\partial^2 T}{\partial x^2}\right) - \mu_{hnf}\left(2\left(\frac{\partial u}{\partial x}\right)^2 + 2\left(\frac{\partial v}{\partial y}\right)^2 + \left(\frac{\partial u}{\partial y} + \frac{\partial \upsilon}{\partial y}\right)^2\right), \tag{3}$$

and subject to the boundary conditions [19]

$$\text{at}\ \ y = 0:\ \ u = U_w = cx,\ \upsilon = 0,\ T = T_w, \tag{4}$$

$$\text{at}\ \ y \to \infty:\ \ u = 0,\ T = T_c, \tag{5}$$

where (u, v) represent the velocity components for (x, y) directions. $\rho, \mu, \rho C_p$ and k exemplify the density, dynamic viscosity, heat capacity, and thermal conductivity, respectively. Subscript of *hnf* represents the hybrid nanofluid, μ_0 is the magnetic permeability, T is temperature, H, and M demonstrate the magnetic field and magnetization, respectively. g represents the gravitational acceleration, β^* is the thermal expansion coefficient and the inclination angle is given by α^*. The first term on the right-hand side in equation (2) represents the component of the ferromagnetic force per unit volume and depends on the existence of the magnetic gradient. In equation (3), the second term on the left-hand side demonstrates the heating due to adiabatic magnetization and viscous dissipation on the last term of the right-hand side [14,23]. The magnetic dipole generates

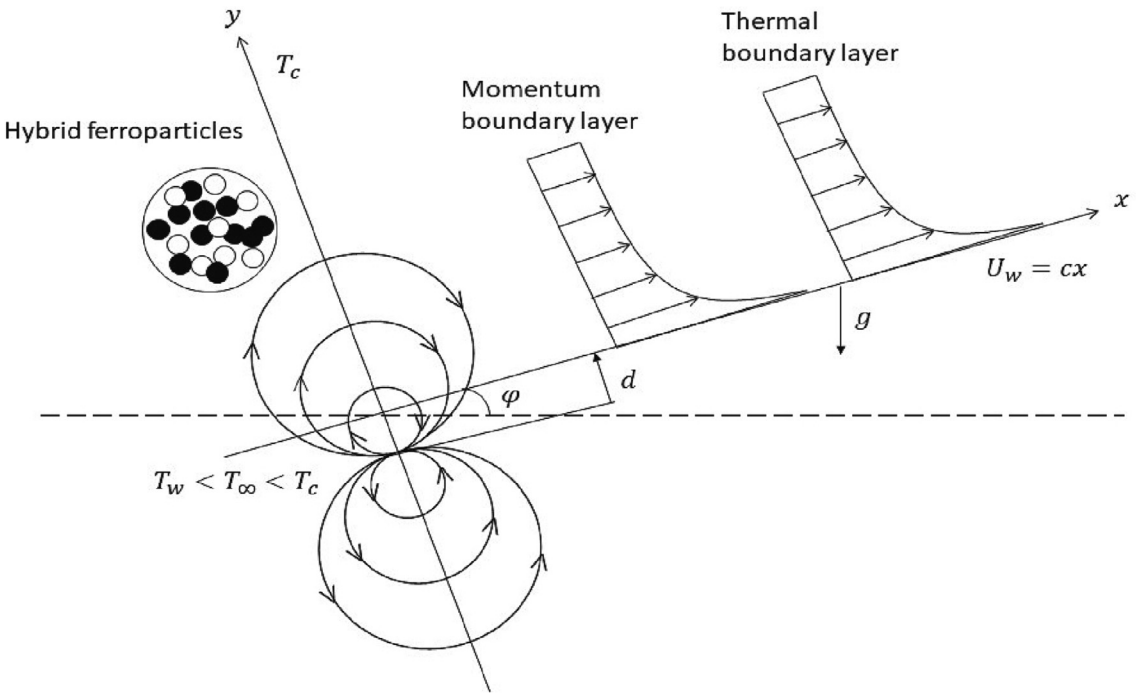

Fig. 1 Physical geometry.

a magnetic field, which influences the flow of the ferrofluid. The magnetic scalar potential can be written [19]

$$\delta = \frac{\gamma}{2\pi}\frac{x}{x^2+(y+d)^2}, \tag{6}$$

where γ represents the magnetic field strength (H) at the source. The H components are of the form [19]

$$\frac{\partial H}{\partial x} = -\frac{\partial \delta}{\partial x} = \frac{\gamma}{2\pi}\frac{x^2-(y+d)^2}{\left(x^2+(y+d)^2\right)^2}, \tag{7}$$

$$\frac{\partial H}{\partial y} = -\frac{\partial \delta}{\partial y} = \frac{\gamma}{2\pi}\frac{2x(y+d)}{\left(x^2+(y+d)^2\right)^2}, \tag{8}$$

because the magnetic body force is proportional to the H gradient, then $H = \sqrt{\left(\frac{\partial \delta}{\partial y}\right)^2 + \left(\frac{\partial \delta}{\partial x}\right)^2}$. By extending equations (7) and (8) in powers of x and considering terms up to order x^2, the components of H may be represented as [19]

$$\frac{\partial H}{\partial x} = -\frac{\gamma}{2\pi}\frac{2x}{(y+d)^2}, \tag{9}$$

$$\frac{\partial H}{\partial y} = \frac{\gamma}{2\pi}\left(-\frac{2}{(y+d)^3} + \frac{4x^2}{(y+d)^5}\right). \tag{10}$$

The linear expression demonstrates the effect of magnetization, M with temperature, T [47] is given as

$$M = -K(T_c - T) \tag{11}$$

where K denotes the thermomagnetic due to the temperature gradient on magnetic materials coefficient. The occurrence of ferrohydrodynamic interaction necessitates two conditions: i) the fluid must have a temperature T different from T_c and ii) an inhomogeneous magnetic field must be applied. The magnetic material loses its magnetization once the ferrofluid reaches the Curie temperature. This property is crucial for practical applications due to the high Curie temperature, which is around 1043 K for iron. Equations (1) to (5) are in the form of PDEs. These equations can be reduced into the set of ODEs by using the following similarity transformations [19]

$$\psi(\xi,\eta) = \left(\frac{\nu}{\rho}\right)\xi f(\eta), \eta = \left(\frac{c\rho}{\mu}\right)^{\frac{1}{2}} y, \xi = \left(\frac{c\rho}{\mu}\right)^{\frac{1}{2}} x,$$

$$\theta(\xi,\eta) = \frac{T_c - T}{T_c - T_w} = \theta_1(\eta) + \xi^2\theta_2(\eta) \tag{12}$$

where ξ, η and $\theta(\xi,\eta)$ are similarity variables and dimensionless temperature, respectively. The stream function $\psi(x,y)$ is defined as $u = \frac{\partial \psi}{\partial y} = cxf'(\eta)$ and $v = -\frac{\partial \psi}{\partial x} = -(c\mu/\rho)^{\frac{1}{2}} f(\eta)$ which automatically satisfies the continuity equation (1). Now, by imposing equation (12) into equations (2) to (3), we have

$$\left(\frac{\mu_{hnf}}{\mu_{bf}}\right)f''' - f'^2 + ff'' - \frac{2\left(\mu_{bf}/\mu_{hnf}\right)\beta\theta_1}{(\eta+\alpha)^4} + \left(\frac{\rho_{hnf}}{\rho_{bf}}\right)\left(\frac{\mu_{hnf}}{\mu_{bf}}\right)\lambda\theta_1 sin\alpha^* = 0, \tag{13}$$

$$\left(\frac{k_{hnf}}{k_{bf}}\right)\left(\theta_1'' + 2\theta_2\right) + \left(\frac{(\rho C_p)_{hnf}}{(\rho C_p)_{bf}}\right)Pr\theta_1' f + \frac{2\chi\beta f(\theta_1 - \varepsilon)}{(\eta+\alpha)^3} - \left(\frac{\mu_{hnf}}{\mu_{bf}}\right)4\chi f'^2 = 0, \tag{14}$$

$$\left(\frac{k_{hnf}}{k_{bf}}\right)\theta_2'' - \left(\frac{(\rho C_p)_{hnf}}{(\rho C_p)_{bf}}\right)Pr(2f'\theta_2 - f\theta_2') + \frac{2\chi\beta f\theta_2}{(\eta+\alpha)^3} - \lambda\beta(\theta_1-\varepsilon)\left[\frac{2f'}{(\eta+\alpha)^4} + \frac{4f}{(\eta+\alpha)^5}\right] - \left(\frac{\mu_{hnf}}{\mu_{bf}}\right)\chi f''^2 = 0, \quad (15)$$

where the Prandtl number (Pr), dimensionless Curie temperature (ε), viscous dissipation (χ), ferrohydrodynamic interaction (β), dimensionless distance (α), and mixed convection number (λ) with Grashof number (Gr_x) and local Reynold number (Re_x). These parameters are defined as

$$Pr = \frac{v}{\alpha}, \varepsilon = \frac{T_\infty}{T_c - T_w}, \chi = \frac{c\mu^2}{\rho k(T_c - T_w)},$$
$$\beta = \frac{\gamma}{2\pi}\frac{\mu_0 K(T_c - T_w)\rho}{\mu^2}, \alpha = \sqrt{\frac{c\rho d^2}{\mu}},$$
$$\lambda = \frac{Gr_x}{Re_x^2} = \frac{\left[\frac{g\beta^*(T_c-T)}{C^2 x}\right]}{Re_x^2} = \frac{g\beta^*(T_c - T)x^3}{v^2}. \quad (16)$$

Boundary conditions (4) and (5) are then reduced to

$$\text{at } \eta = 0 : f(\eta) = 0, f'(\eta) = 1, \theta_1(\eta) = 1, \theta_2(\eta) = 0, \quad (17)$$

$$\text{at } \eta \to \infty : f'(\eta) \to 0, \theta_1(\eta) \to 0, \theta_2(\eta) \to 0. \quad (18)$$

Ethylene glycol plus water as proposed by [32,33] is used as the base fluid for the Newtonian ferrofluid together with spherical-shaped hybrid ferroparticles of Fe_3O_4 and $CoFe_2O_4$. Ethylene glycol plus water is the Newtonian fluid since its viscosity is constant when the shear rate is increased [49]. The spherical particles have small particles with a high surface area. The smaller particles have a low sedimentation rate and energy levels. Table 1 illustrates the thermophysical properties of the base fluid and nanoparticles at an ambient temperature of 25℃ [48]. The thermophysical properties of the hybrid ferrofluid are presented in Table 2. Here, the superscript of nf, bf, s_1, s_2 and ϕ represent the ferrofluid, base fluid, first solid ferroparticles (Fe_3O_4), second solid ferroparticles ($CoFe_2O_4$), and nanoparticle's volume fraction, respectively.

The local skin friction, C_f and Nusselt number, Nu_x are defined as [19]

$$C_f = -\frac{2\tau_w}{\rho_{bf}U_w^2}, \text{ and } Nu_x = \frac{xq_w}{k_{bf}(T_c - T_w)} \quad (19)$$

which depicts the wall shear stress, $\tau_w(x)$ and heat transfer rate, $q_w(x)$, respectively. These physical interests can be defined as

Table 1 Base fluid and nanoparticles thermophysical characteristics [40,48].

Properties	Ethylene glycol (50%) plus water (50%)	Fe_3O_4	$CoFe_2O_4$
$\rho(kgm^{-3})$	1056	5180	4907
$C_p(Jkg^{-1}K^{-1})$	3.288	670	700
$k(Wm^{-1}K^{-1})$	0.425	9.7	3.7
Pr	29.86	–	–

$$\tau_w = \mu_{hnf}\left.\frac{\partial u}{\partial y}\right|_{y=0} \text{ and } q_w = -k_{hnf}\left.\frac{\partial T}{\partial y}\right|_{y=0}. \quad (20)$$

By applying the similarity equation (12), the dimensionless local skin friction and heat transfer coefficients are written as [23,31]

$$C_f Re_x^{\frac{1}{2}} = -\frac{2}{\mu_{hnf}} f''(0) and Re_x^{-\frac{1}{2}} Nu_x = -\frac{k_{hnf}}{k_{bf}}\left[\theta_1'(0) + \xi^2\theta_2'(0)\right]. \quad (21)$$

3. Numerical method

The Keller box method, an implicitly stable numerical approach, is employed to solve the governing equations (13) to (15) as well as the boundary conditions (17) to (18). The method has been found to be particularly accurate for nonlinear problems. It must be emphasized once more that this numerical scheme has proven to be easier, more adaptable, and more effective to use than the majority of other numerical approaches, including the local nonsimilarity method, and to provide numerical results with a high degree of accuracy. More importantly, the method is numerically stable, enabling calculations to be performed [50]. Following the four primary steps lead to a numerical solution.

3.1. First-order system

Equations (13) to (15) reduce to a first-order system by introducing the new dependent variables $f = f, f' = u, f'' = v, \theta_1 = \theta, \theta_1' = s, \theta_2 = g, \theta_2' = w$, obtained

$$\left(\frac{\mu_{hnf}}{\mu_{bf}}\right)v' - u^2 + fv - \frac{2(\mu_{bf}/\mu_{hnf})\beta\theta}{(\eta+\alpha)^4} + \left(\frac{\rho_{hnf}}{\rho_{bf}}\right)\left(\frac{\mu_{hnf}}{\mu_{bf}}\right)\lambda\theta sin\alpha^* = 0, \quad (22)$$

$$\left(\frac{k_{hnf}}{k_{bf}}\right)(s' + 2g) + \left(\frac{(\rho C_p)_{hnf}}{(\rho C_p)_{bf}}\right)Prsf + \frac{2\chi\beta f(\theta-\varepsilon)}{(\eta+\alpha)^3} - \left(\frac{\mu_{hnf}}{\mu_{bf}}\right)4\chi u^2 = 0, \quad (23)$$

$$\left(\frac{k_{hnf}}{k_{bf}}\right)w' - \left(\frac{(\rho C_p)_{hnf}}{(\rho C_p)_{bf}}\right)Pr(2ug - fw) + \frac{2\chi\beta fg}{(\eta+\alpha)^3} - \lambda\beta(\theta-\varepsilon)\left[\frac{2u}{(\eta+\alpha)^4} + \frac{4f}{(\eta+\alpha)^5}\right] - \left(\frac{\mu_{hnf}}{\mu_{bf}}\right)\chi v^2 = 0, \quad (24)$$

3.2. Finite difference scheme

The rectangular grid in the $x - \eta$ plane is shown in Fig. 2 and the net points are

Table 2 Base fluid and ferroparticles thermophysical characteristics [40].

Properties	Hybrid nanofluid
Viscosity	$\mu_{hnf} = \frac{\mu_{bf}}{(1-\phi_1)^{2.5}(1-\phi_2)^{2.5}}$
Density	$\rho_{hnf} = (1-\phi_2)\left[(1-\phi_1)\rho_{bf} + \phi_1\rho_{s_1}\right] + \phi_2\rho_{s_2}$
Specific heat capacity	$(\rho C_p)_{hnf} = (1-\phi_2)\left[(1-\phi_1)(\rho C_p)_{bf} + \phi_1(\rho C_p)_{s_1}\right] + \phi_2(\rho C_p)_{s_2}$
Thermal conductivity	$k_{hnf} = \frac{k_{s_2}+2k_{nf}-2\phi_2(k_{nf}-k_{s_2})}{k_{s_2}+2k_{nf}+\phi_2(k_{nf}-k_{s_2})} \times k_{nf}$where $\frac{k_{nf}}{k_{bf}} = \frac{k_{s_1}+2k_{bf}-2\phi_2(k_{bf}-k_{s_1})}{k_{s_1}+2k_{bf}+\phi_2(k_{bf}-k_{s_1})}$

$$x^0 = 0, x^i = x^{i+1} + k_i, i = 1, 2, 3, \cdots I,$$

$$\eta_0 = 0, \eta_j = \eta_{j+1} + h_j, j = 1, 2, 3, \cdots J,$$

where k_i and h_j are the Δx and $\Delta\eta$ -spacing, respectively. i and j are the sequence of numbers that indicate the coordinate location. Generally, the derivatives in the $\eta-$ direction are defined as

$$[\ ]' = \frac{\partial[\ ]}{\partial\eta} = \frac{[\ ]_j - [\ ]_{j-1}}{h_j}, \tag{25}$$

and for any point

$$[\ ]_{j-\frac{1}{2}} = \frac{1}{2}\left([\ ]_j - [\ ]_{j-1}\right). \tag{26}$$

The finite difference is generated by imposing the derivatives of (25) and (26) on the first-order derivatives presented in the preceding subsection. While equations (22) to (24) are approximated by the central difference scheme at the midpoint $\left(x^i, \eta_{j-\frac{1}{2}}\right)$. The associated boundary conditions (17) to (18) at $x = x^i$ are

$$f_0^i = 0, u_0^i = 0, \theta_0^i = 0, g_0^i = 0 \tag{27}$$

$$u_J^i = 0, \theta_J^i = 0, g_J^i = 0. \tag{28}$$

3.3. Newton's method

The resulting equations after applying the finite difference method are nonlinear algebraic system equations. Newton's approach is used to linearize the nonlinear system by introducing the iterates for the new dependent variables.

3.4. Block elimination method

The block tri-diagonal factorization scheme is employed to solve the matrix of the linear system. A block tri-diagonal matrix is a special block matrix since it consists of a block of matrices. The matrix is written as $[A][\delta] = [r]$, where matrix A is zero excluding those three along the diagonal. The solutions are obtained by solving the matrix using the block-elimination method (Thomas algorithm). The calculation of the value δ is repeated until it satisfies $\left|\delta v_0^{(i)}\right| \leq \varepsilon$ with $\varepsilon = 0.00001$ to achieve four decimal accuracies for most predicted quantities. A comprehensive description of the

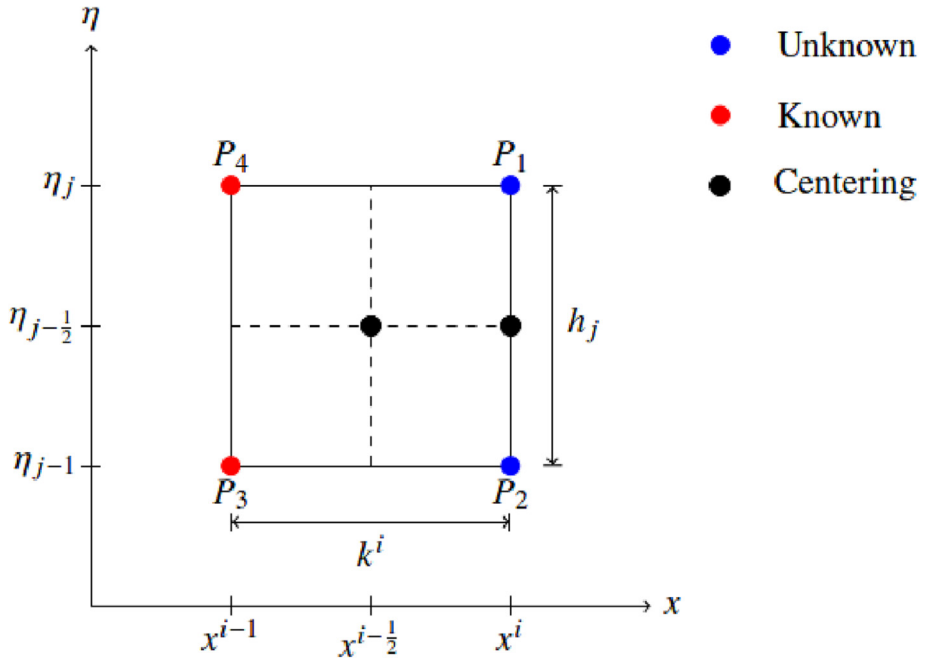

Fig. 2 Net rectangle for difference approximation.

approach can be found in Cebeci and Bradshaw [51] and Malik *et al.*[52].

4. Results and discussion

The main purpose of the current study is to analyze the behavior of the hybrid ferrofluid, $Fe_3O_4 - CoFe_2O_4$ which dissolved in ethylene glycol plus water as the base fluid numerically under the effect of the magnetic dipole at different inclination angles. Figures and tables are employed to describe the examined characteristics, which include ferromagnetic (β), ferroparticles volume fraction (ϕ_2), and mixed convective parameter (λ) by considering three cases namely, $\alpha^* = 0$ (horizontal stretching sheet), $\alpha^* = \frac{\pi}{8}$ (inclination angle), and $\alpha^* = \frac{\pi}{4}$ (vertical stretching sheet). Through this study, the permanent parameters by Andersson and Valnes [19] are set as the initial study: $\varepsilon = 2.0, \chi = 0.01$ and $\alpha = 1.0$.

4.1. Verification of the results

The current method is validated by comparing the obtained numerical results with previous publications. Fig. 3 illustrates a comparison between the numerical results obtained through the Keller box method and the previous findings reported by [20,23]. It is noticed that the special case of the current study is discovered to be in amazing concurrence with the distributed results given by Andersson and Valnes [19]. In addition, Table 3 demonstrates an excellent agreement of the numerical results with the studies reported by Olanrewaju [10], Zeeshan and Majeed [22], and Punith *et al.* [24].

4.2. Inclination angle(α^*)

The effect of the inclination angles is designated in Fig. 4 for the velocity profile and Fig. 5 for the temperature profile. Increasing the inclination angle from 0 to $\frac{\pi}{3}$ leads to suppressing the velocity profile. Physically, the gravitational force component acting along the surface gets more pronounced as the stretch sheet's angle increases. This leads to a greater pressure difference along the surface. At $\alpha^* = 0$, it depicts the scenario of a horizontal sheet with no gravitational force in the fluid. The greatest gravitational force companionship occurs as the sheet goes from horizontal to vertical direction by changing the values of α^* from 0 to $\frac{\pi}{3}$ Consequently, the intensity of buoyant forces in the fluid increases which enhances natural convection by a factor of $sin\alpha^*$. Due to variations in the locations of the aligned angles, the aligned magnetic field behaves like a transverse magnetic field for $\frac{\pi}{4}$ and attracts the nanoparticles. This can drive more vigorous fluid motion hence, the fluid particles will freely flow and the momentum barrier layer will form distant from the sheet. As the sheet changes from a horizontal to a vertical plate, the thermal boundary layer cools down, while the inclination angle results in a delay in the temperature profile. The reason for this is that as the angle of inclination of the sheet elevates from forced convection to mixed convection to natural convection, the effective surface area exposed to the fluid shrinks. Heat transmission is proportional to the surface area available for heat exchange. A decreased surface area means less contact between the sheet and the fluid, resulting in a slower heat transfer rate. The temperature of the fluid will normally be lower as less heat is delivered to it. The identical action of both profiles has been proven by the study of Titus and Abraham [21] and Zeeshan *et al.* [22]. The outcome clearly shows that altering the stretching sheet's angles may significantly affect the temperature of the hybrid ferrofluid in the cooling and heating process including cancer treatment.

4.3. Ferrohydrodynamic interaction(β)

Figs. 6 and 7 are plotted to depict the velocity profile $f'(\eta)$ and temperature profile $\theta_1(\eta)$ for different values of β. The analysis

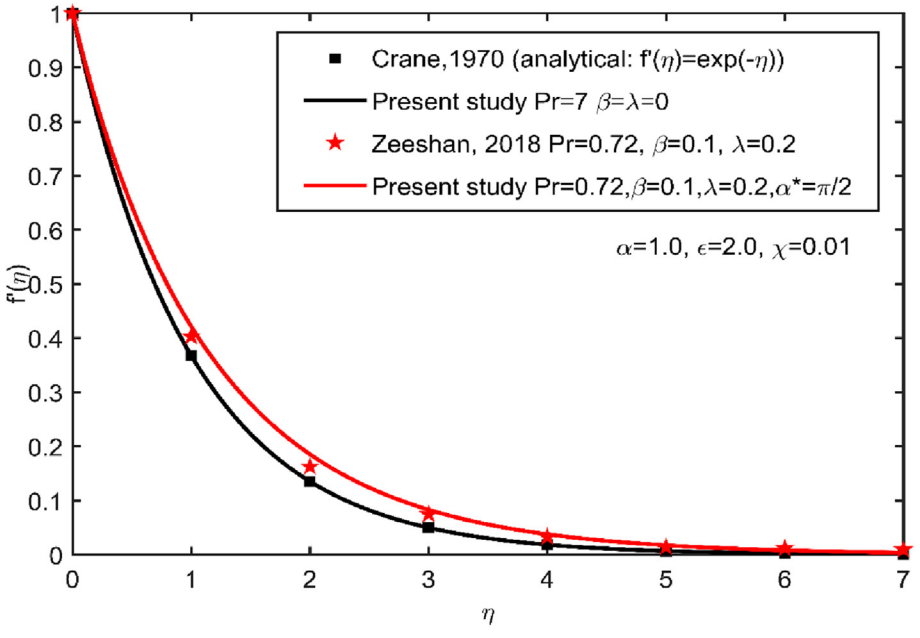

Fig. 3 Verification of the current results.

Table 3 Comparison of $-f''(0)$.

Published paper	Olanrewaju [10]	Zeeshan and Majeed [22]	Punith *et al.* [24]	Present result
$-f''(0)$	0.605848	0.6058427	0.6069352	0.6069

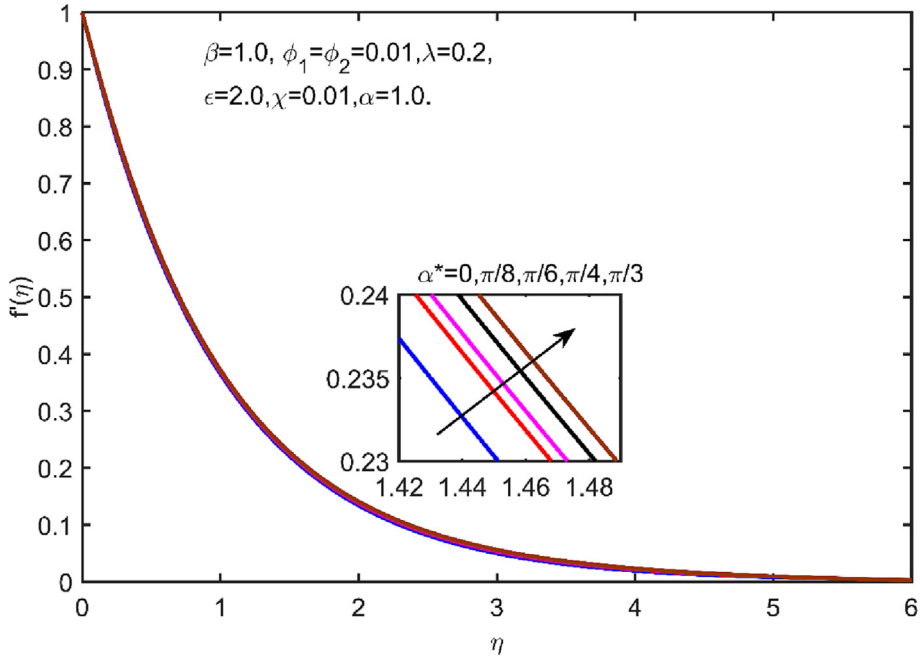

Fig. 4 $f'(\eta)$ for sundry parameters of α^*.

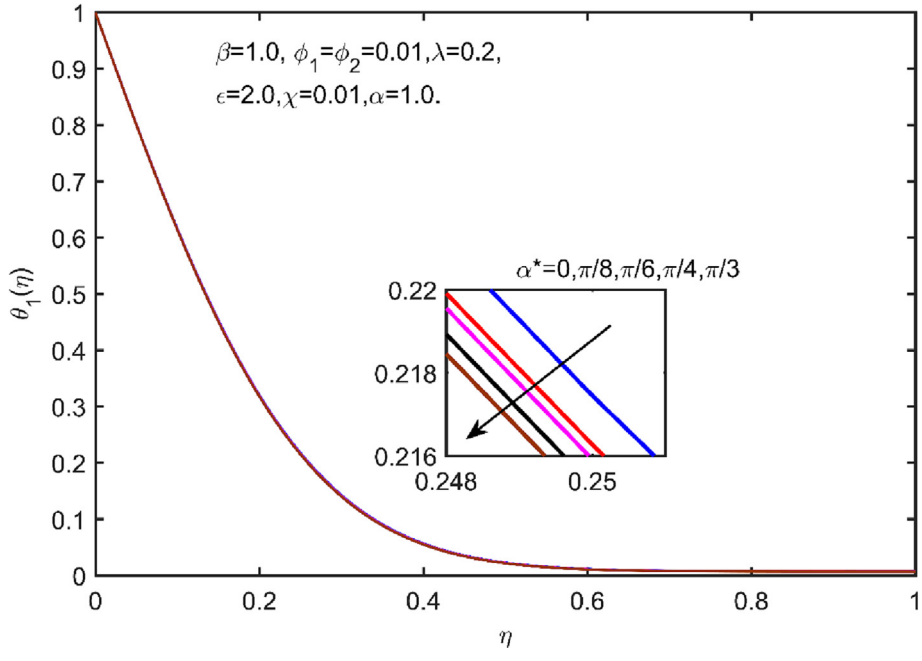

Fig. 5 $\theta_1(\eta)$ for sundry parameters of α^*.

is carried out by setting β from 1 to 5 [23]. The magnetic field strength exists owing to the magnetic dipole's location under the sheet, which generates the ferromagnetic effect on the boundary layer ferrofluid flow. Because the ferrofluid is magnetic in nature, the existence of a magnetic dipole interferes with the fluid movement of the ferroparticle owing to magnetic attraction to the ferroparticle, worsening the fluid's viscosity. According to equation (16), when the values of the parameter β increase, the magnetic field that the magnetic dipole produces becomes stronger. Therefore, it leads to a slight reduction in the velocity of the fluid in a hybrid ferrofluid, as depicted in Fig. 6. It is interesting to note that the momentum boundary layer thickness approaches the elastic sheet, thereby turning thinner. The increment of the viscosity leads to an upsurge in the frictional force in the hybrid ferrofluid. The presence of such force in the hybrid ferrofluid suppresses the collision rate between particles and then, converts mechanical energy (potential energy and kinetic energy) into thermal energy. Hence, it enhances the temperature profile as well as the thermal boundary layer as illustrated in Fig. 7. This observation shows that an exceeding magnetic field can result in a more severe temperature rise, which is essential for efficiently destroying cancer cells via hyperthermia treatment. In the current challenge, the velocity and temperature characteristics of the hybrid ferrofluid when embedded with various values of parameter β have exhibited similar behavior as observed by Andersson and Valnes [19] (ferrofluid) and Zeeshan *et al.* [22,23,31] (nano-ferrofluid).

In comparison to an incline $\left(\alpha^* = \frac{\pi}{8}\right)$ and a vertical stretching sheet $\left(\alpha^* = \frac{\pi}{4}\right)$, the particle mobility of the hybrid ferrofluid decomposes more with a horizontal stretching sheet. This emerges because the fluid's viscosity cannot be overcome by forced convection due to ferrohydrodynamic processes. As a result, fluid particles travel relatively slowly in comparison to natural convection and mixed convection owing to buoyancy force dominating. When the temperature of the hybrid ferrofluid on the vertical sheet is compared to that on other angles, such as the incline and horizontally stretched sheet, it is observed to be lower. This is because the buoyancy force creates a convection flow, which serves to cool down the ferrofluid. Interestingly, in the absence of buoyancy when stretching the sheet horizontally, the heat content in the liquid is at its maximum consistent with the thermal conductivity under the FHD effect.

4.4. Ferroparticles volume fraction(ϕ_2)

Fig. 8 demonstrates the changes in the velocity profile caused by an increase in the volume fraction ϕ_2 of ferroparticles. The output of the total ferroparticles volume fraction (ϕ_{hnf}) is applied up to 4% due to the Brinkman model in Table 2. From this figure, the behavior of that profile depicts that the suspension of the ferroparticles eliminates the velocity movement by lowering the momentum boundary layer. When the fluid is robust with the ferroparticles, the viscous rate in the fluid slightly raises causing the inflation of the frictional force in the hybrid ferroparticles. Consequently, such a force restricts the rate of collision among the ferroparticles and additionally prompts the velocity profile to diminish. Fig. 8 depicts stretched sheets ranging from horizontal to vertical by varying the values of the parameter α^*. As the concentration of ferroparticles grows, the velocity profile in forced convection tends to fall more severely than in mixed and natural convection. This indicates that the lowest buoyancy force in forced convection leads the particles to be in a tight and compact configuration thereby, slowing their motion. In short, the lowering of the inclination angle prohibits the particles from moving freely.

The accumulation of ferroparticles in the fluid led to an improvement in its temperature, as evidenced by Fig. 9. This

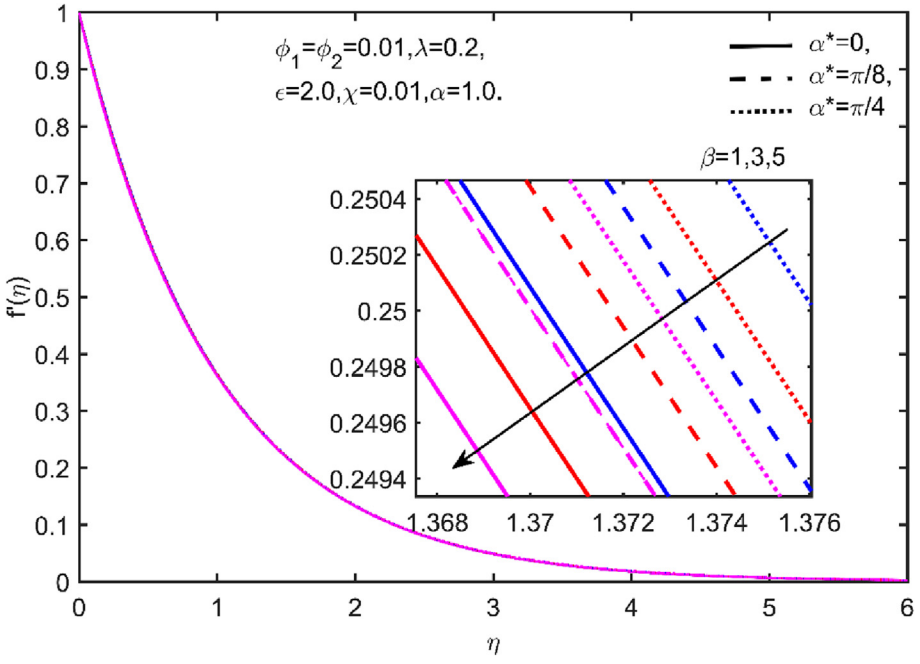

Fig. 6 $f'(\eta)$ for sundry parameters of β.

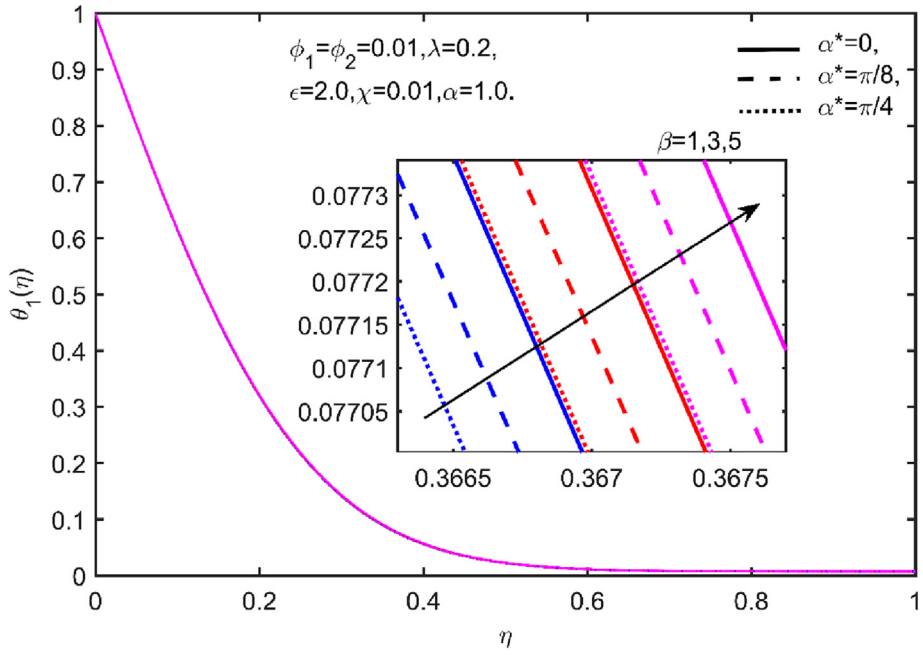

Fig. 7 $\theta_1(\eta)$ for sundry parameters for β.

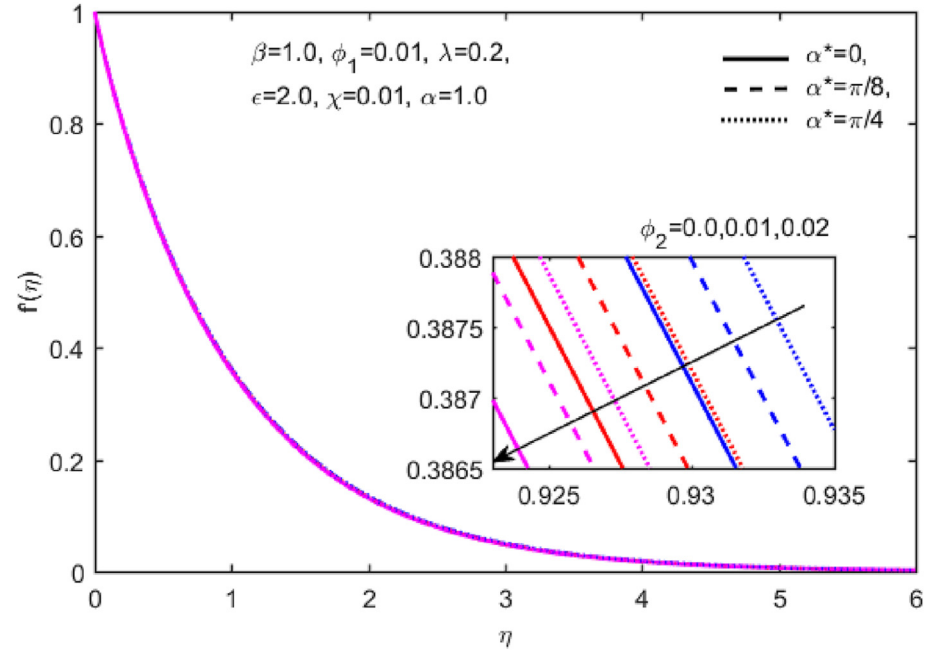

Fig. 8 $f'(\eta)$ for sundry parameters of ϕ_2.

is attributed to the ferroparticles' ability to increase the thermal conductivity of the fluid. In this way, more heat energy will be consumed and simultaneously causes an increment in the thickness of the thermal boundary layer. The results coincide with the results obtained by Muhammad *et al.* [28–30] who investigated the ferrite nanoparticles in a liquid including ethylene glycol as the base fluid. It is interesting to mention that this rise in temperature is essential for hyperthermia therapy because it can cause cancer cells to suffer thermal damage, which eventually kills them. It is inferred from Fig. 9 that the temperature profile fell as the angle of the sheet increased. It means that the scarcity of buoyancy force passing through the horizontal sheet when $\alpha^* = 0$ assists in heat storage and the fluid will be hotter than the vertical sheet when $\alpha^* = \frac{\pi}{4}$. The hybrid ferrofluid flow over a solid surface by the external agencies during forced convection enhanced the heat transfer leading to improve temperature in the fluid. The presence of the buoyancy force either in mixed or natural convection causes the particles of the fluid to move upward and far away from the sheet. Basically, the buoyancy force, commonly

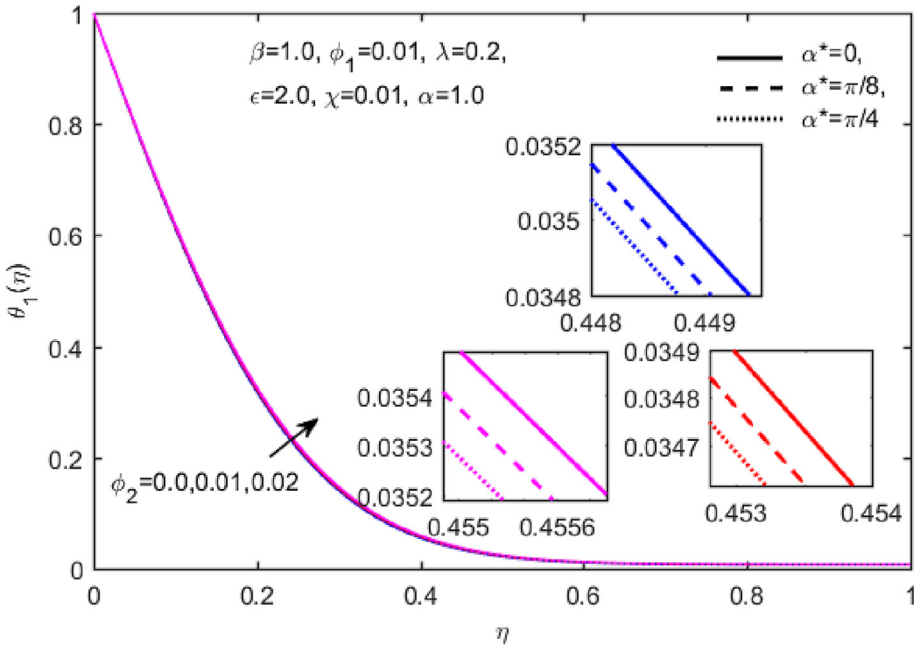

Fig. 9 $\theta_1(\eta)$ for sundry parameters of ϕ_2.

known as Archimedes' principle, is the upward force produced on a floating item owing to the density differential between the object and the surrounding fluid. As a result, the heat generated during sheet stretching is not entirely absorbed by the fluid particles, resulting in a reduced thermal field as compared to forced convection.

4.5. Mixed convective parameter(λ)

Fig. 10 reveals the velocity profile against the various values of parameter λ. It is detected that the hybrid ferroparticles move away from the stretching sheet and result in surging the velocity profile with an increase in parameter λ. This can be caused by the fact that according to the last dimensionless parameter in equation (16), λ speak for the ratio of the local Grashof number (Gr_x) and Reynold's number (Re_x). Gr_x illuminates the ratio of buoyancy force to the viscous force. Gr_x is inversely proportional to viscous force but directly proportional to the buoyant force. The growth of the buoyancy force rather than the viscous force as λ increased enables the ferroparticles to move speedier thereby, thicker the momentum boundary layer. The behavior of the temperature profile against λ is plotted in Fig. 11. The temperature distribution retails with an augment in the value of λ. Incrementation of the buoyancy forces colds down the hybrid ferrofluid by lessening the thermal boundary layer. Furthermore, the velocity profile remains constant when $\lambda = 0$ in all circumstances because the last part of the momentum equation (13) becomes a limiting case of the stretched sheet in the absence of buoyancy force. Titus and Abraham [21] and Zeeshan *et al.* [22] also claimed similar characteristics of velocity and temperature fields of electrically nonconducting ferrofluid.

The velocity of the fluid is greater in the vertical case $\left(\alpha^* = \frac{\pi}{4}\right)$ with the highest buoyancy force when compared to the case of $\alpha^* = \frac{\pi}{8}$ but in the opposite direction for the temperature field. The ratio of $Gr_x/Re_x^2 \gg 1$ demonstrates natural convection, if the $Gr_x/Re_x^2 \ll 1$ indicates forced convection and the combination of forced and free convection must be considered if $Gr_x/Re_x^2 \approx 1$ [53]. Hence, the higher of Gr_x/Re_x^2 in natural convection compared to mixed convection as well as forced convection drag to improve the buoyancy force in the hybrid ferrofluid. When a fluid is heated, the particles of the hybrid ferrofluid become less dense, allowing them to float easily with the assistance of maximal buoyancy force, whilst the particles in the colder section drop due to their higher density. This density differential creates a circulation pattern, resulting in a fluid motion. As the heated fluid rises, the fluid velocity near the heated surface increases, leading to an upward flow and providing a higher velocity profile. With an overall reduction in parallel buoyancy to the surface, there is a diminish in fluid velocity down the plate, which happens in a forced convection state. Conversely, when the ratio of Gr_x to Re_x^2 approaches one, the heat content during sheet stretching is minimized. As a consequence, the temperature at the sheet during mixed convection is considerably lower than the ambient temperature and the Curie temperature of the magnetic material when the sheet is extended.

4.6. Local skin friction and Nusselt number

Table 4 shows the changes in local skin friction $C_f Re_x^{\frac{1}{2}}$ and Nusselt number $Nu_x Re_x^{-\frac{1}{2}}$ for the various investigated parameters in three cases namely, $\alpha^* = 0$ (horizontal stretching sheet), $\alpha^* = \frac{\pi}{8}$, (incline sheet) and $\alpha^* = \frac{\pi}{4}$ (vertical stretching sheet). The pattern for the various values of β coincides with the results of initial work on ferrofluids reported by Andersson and Valnes [19] in both physical quantities. An increase in the ferrohydromagnetic interaction upsurges the local skin friction but eliminates the Nusselt number. The greatest buoyancy force at the vertical sheet tends to enhance the shear stress

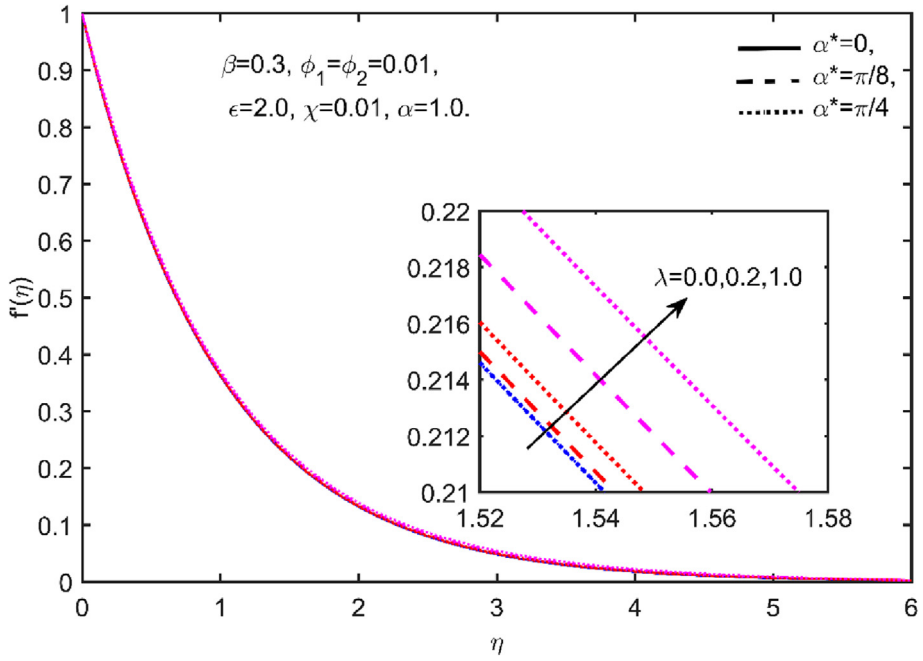

Fig. 10 $f'(\eta)$ for sundry parameters of λ.

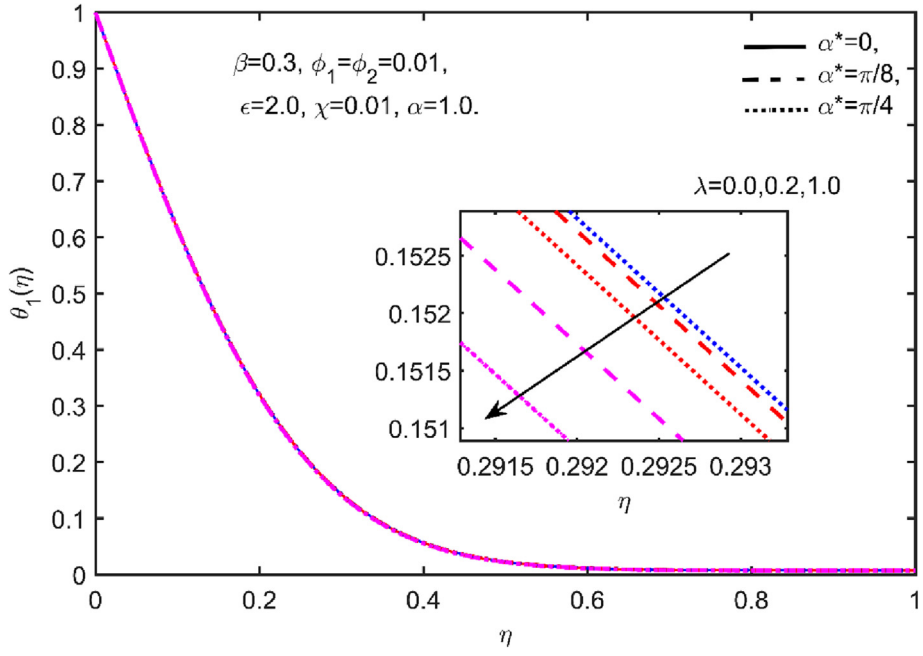

Fig. 11 $\theta_1(\eta)$ for sundry parameters of λ.

by 62.88% when compared to cases $\alpha^* = \frac{\pi}{8}$, 62.42% and $\alpha^* = 0$, 61.87%. The incrementation of the conductive heat transfer and the reduction in the convective heat transfer is detected in hybrid ferrofluid pass through the horizontal stretching sheet when the values of $Nu_x Re_x^{-\frac{1}{2}}$ declines by 9.86% followed by 9.85% for $\alpha^* = \frac{\pi}{8}$ and 9.84% for vertically stretched sheets. Therefore, the ferrohydromagnetic interaction parameter may improve the heat transfer of the hybrid in the circumstance without gravity and buoyant forces during forced convection.

Further, $C_f Re_x^{\frac{1}{2}}$ boost immensely when the values of the concentration of nanoparticles volume fraction were enhanced. As more nanoparticles are added to the fluid, the fluid flow becomes increasingly distorted, which in turn escalates the level of shear stress experienced by the fluid. A similar trend has been observed by Zainodin *et al.*[40] that analyzed mixed convection hybrid ferrofluid flow, $Fe_3O_4 - CoFe_2O_4$. The domination of $Nu_x Re_x^{-\frac{1}{2}}$ drop off as it intensifies the concentration of ϕ_2 and in line with the expected output as in

Table 4 $C_f Re_x^{\frac{1}{2}}$ and $Nu_x Re_x^{-\frac{1}{2}}$ for β, ϕ_2 and λ.

β	ϕ_2	λ	$\alpha^* = 0$		$\alpha^* = \frac{\pi}{8}$		$\alpha^* = \frac{\pi}{4}$	
			$-C_f Re_x^{\frac{1}{2}}$	$-Nu_x Re_x^{-\frac{1}{2}}$	$-C_f Re_x^{\frac{1}{2}}$	$-Nu_x Re_x^{-\frac{1}{2}}$	$-C_f Re_x^{\frac{1}{2}}$	$-Nu_x Re_x^{-\frac{1}{2}}$
1			1.1917	3.8636	1.1804	3.8654	1.1708	3.8668
3			1.5573	3.6707	1.5456	3.6726	1.5358	3.6741
5			1.9291	3.4827	1.9172	3.4846	1.9071	3.4863
	0.00		1.1911	3.8943	1.1799	3.8960	1.1704	3.8974
	0.01		1.1917	3.8636	1.1804	3.8654	1.1708	3.8668
	0.02		1.1918	3.8371	1.1806	3.8389	1.1712	3.8403
		0.0	1.0643	3.9359	1.0643	3.9359	1.0643	3.9359
		0.2	1.0643	3.9359	1.0586	3.9368	1.0435	3.9390
		1.0	1.0643	3.9359	1.0081	3.9443	0.9608	3.9513

Ramesh *et al.* [39]. For raising the concentration of $CoFe_2O_4$, it has been discovered that forced convection has a larger shear stress than mixed convection and natural convection. However, the heat transfer rate on natural convection improves the heat transfer rate. Consequently, natural convection hybrid ferrofluid flow across a vertical stretch sheet can assist a system's cooling process.

Furthermore, the effect of mixed convective possessed a negative effect on the wall shear stress where the values of $C_f Re_x^{\frac{1}{2}}$ falls for both cases, $\alpha^* = \frac{\pi}{8}$ and $\alpha^* = \frac{\pi}{4}$. A significant percentage decrease occurs at $\alpha^* = \frac{\pi}{4}$ (9.72%) when the buoyancy effect is higher than the gravitational force followed by 5.28% when $\alpha^* = \frac{\pi}{8}$. On the other hand, an opposite trend is observed for $Nu_x Re_x^{-\frac{1}{2}}$. When the hybrid ferrofluid flows at stronger buoyancy forces, heat transmission rises, emphasizing convective heat transfer over conductive heat transfer. The percentage increments for $\alpha^* = \frac{\pi}{8}$ and $\alpha^* = \frac{\pi}{4}$ are 0.21% and 0.38%, respectively. The observed behavior of the ferromagnetic flow due to the mixed convection parameter corresponding to the local skin friction and Nuselt number are comparable to the results achieved in Zeeshan *et al.* [23].

The effect of inclination angles for $C_f Re_x^{\frac{1}{2}}$ and $Nu_x Re_x^{-\frac{1}{2}}$ are declared in Table 5. From this table, it is evident that the increase of the inclination angles tends to decline the shear stress but enhance the changes of heat transfer. This is because the maximum buoyancy force is responsible for improving the $Nu_x Re_x^{-\frac{1}{2}}$ of the hybrid ferrofluid. According to the results, $C_f Re_x^{\frac{1}{2}}$ decays significantly due to the buoyancy force which inhibits the deformation of the hybrid ferrofluid to flow optimally. Surprisingly, when the buoyancy force is at its peak in natural convection, the variations in heat transmission rise.

Table 5 $C_f Re_x^{\frac{1}{2}}$ and $Nu_x Re_x^{-\frac{1}{2}}$ for z.

α^*	$-C_f Re_x^{\frac{1}{2}}$	$-Nu_x Re_x^{-\frac{1}{2}}$
0	1.0643	4.0295
$\frac{\pi}{8}$	1.0081	4.0379
$\frac{\pi}{6}$	0.9910	4.0405
$\frac{\pi}{4}$	0.9608	4.0449
$\frac{\pi}{3}$	0.9378	4.0483

5. Conclusions

In this work, we studied and discussed the influence of hybrid ferroparticles, $Fe_3O_4 - CoFe_2O_4$, with a magnetic dipole on the heat transfer of ethylene glycol plus water toward an inclined stretching. The governing equation was solved using a finite difference method scheme via the Keller box method in MATLAB software. The physical properties of the hybrid magnetic nanofluid were affected by different values of the inclination angles, ferrohydrodynamic interaction, ferroparticles volume fraction, and mixed convection parameter, which had an impact on the temperature profile, velocity field, skin friction coefficient, and heat transfer rate. By adjusting the angle of the inclination sheet, the behavior of the heat transfer flow considers three heat transfer mechanisms: free or natural convection, forced convection, and mixed convection. The main findings of this problem are listed below;

i. The natural convection improved fluid velocity by expanding the inclination angle parameter. This was attributed to the peak buoyancy force in natural convection, allowing the particles to flow freely. However, forced convection, which lacks buoyancy or gravitational force, enhanced the temperature field beyond mixed and natural convection.
ii. When α^* varies from 0 to $\frac{\pi}{3}$, the shear stress decreased by 11.89% and rapid increase in the heat transfer rate of approximately 0.47%.
iii. Despite the magnetic dipole effect reducing fluid velocity, it raised the temperature of the hybrid ferrofluid in the heat transfer system.
iv. When β varies from 1 to 5, the increment of local skin friction for $\alpha^* = 0, \alpha^* = \frac{\pi}{8}$, and $\alpha^* = \frac{\pi}{4}$ are 61.87%, 62.42%, and 62.88%, respectively.
v. When β varies from 1 to 5, the decrement of the Nusselt number for $\alpha^* = 0, \alpha^* = \frac{\pi}{8}$, and $\alpha^* = \frac{\pi}{4}$ are 9.86%, 9.85% and 9.84%, respectively.
vi. In particular, $CoFe_2O_4$ acted as an insulator by increasing the concentration of ferroparticles, resulting in a reduction in the rate of heat transmission.

vii. The velocity profile for the mixed convection parameter exhibited a different pattern compared to the temperature profile, which was influenced by the varying value ratios of the local Grashof number and Reynold's number.
viii. The results of this study are highly relevant for the cooling and heating process, particularly in the treatment of cancer using hyperthermia.

Declaration of Competing Interest

The authors declare that they have no known competing financial interests or personal relationships that could have appeared to influence the work reported in this paper.

Acknowledgments

This research was funded by a grant from the Ministry of Higher Education of Malaysia (FRGS Grant FRGS/1/2021/STG06/UTM/02/6) and Universiti Teknologi Malaysia through vote number 08G33.

References

[1] B. Jalili et al, Thermal analysis of Williamson fluid flow with Lorentz force on the stretching plate, Case Stud. Therm. Eng. 39 (2022) 102374.
[2] B. Iftikhar, M.A. Siddiqui, T. Javed, Dynamics of magnetohydrodynamic and ferrohydrodynamic natural convection flow of ferrofluid inside an enclosure under non-uniform magnetic field, Alex. Eng. J. 66 (2023) 523–536.
[3] M. Murtaza, E. Tzirtzilakis, M. Ferdows, Effect of electrical conductivity and magnetization on the biomagnetic fluid flow over a stretching sheet, Z. Angew. Math. Phys. 68 (2017) 1–15.
[4] B. Jalili et al, Squeezing flow of Casson fluid between two circular plates under the impact of solar radiation, ZAMM-Journal of Applied Mathematics and Mechanics/Zeitschrift für Angewandte Mathematik und Mechanik (2023) e202200455.
[5] P. Jalili et al, Heat transfer analysis in cylindrical polar system with magnetic field: A novel Hybrid Analytical and Numerical Technique, Case Stud. Therm. Eng. 40 (2022) 102524.
[6] P. Jalili et al, A novel analytical approach to micro-polar nanofluid thermal analysis in the presence of thermophoresis, Brownian motion and Hall currents, Soft. Comput. 27 (2) (2023) 677–689.
[7] P. Jalili et al, Study of nonlinear radiative heat transfer with magnetic field for non-Newtonian Casson fluid flow in a porous medium, Results Phys. 48 (2023) 106371.
[8] S. Li et al, Effects of activation energy and chemical reaction on unsteady MHD dissipative Darcy-Forchheimer squeezed flow of Casson fluid over horizontal channel, Sci. Rep. 13 (1) (2023) 2666.
[9] S. Mamatha et al, Multi-linear regression of triple diffusive convectively heated boundary layer flow with suction and injection: Lie group transformations, Int. J. Mod Phys B 37 (01) (2023) 2350007.
[10] P. Olanrewaju, Effects of internal heat generation on hydromagnetic non-Darcy flow and heat transfer over a stretching sheet in the presence of thermal radiation and ohmic dissipation, World Appl. Sci. J. 16 (2012) 37–45.
[11] R.E. Rosensweig, *Ferrohydrodynamics*, Courier Corporation, 2013.
[12] B.D. Cullity, C.D. Graham, Introduction to magnetic materials, John Wiley & Sons, 2011.
[13] K. Seleznyova, M. Strugatsky, J. Kliava, Modelling the magnetic dipole, Eur. J. Phys. 37 (2) (2016) 025203.
[14] J.L. Neuringer, R.E. Rosensweig, Ferrohydrodynamics, Phys. Fluids 7 (12) (1964) 1927–1937.
[15] L. Vékás, Ferrofluids and magnetorheological fluids, Advances in science and technology, Trans Tech Publ, 2008.
[16] M. Lajvardi et al, Experimental investigation for enhanced ferrofluid heat transfer under magnetic field effect, J. Magn. Magn. Mater. 322 (21) (2010) 3508–3513.
[17] L.S. Arias et al, Iron oxide nanoparticles for biomedical applications: A perspective on synthesis, drugs, antimicrobial activity, and toxicity, Antibiotics 7 (2) (2018) 46.
[18] S.R. Mokhosi et al, Advances in the Synthesis and Application of Magnetic Ferrite Nanoparticles for Cancer Therapy, Pharmaceutics 14 (5) (2022) 937.
[19] H. Andersson, O. Valnes, Flow of a heated ferrofluid over a stretching sheet in the presence of a magnetic dipole, Acta Mechanica 128 (1) (1998) 39–47.
[20] L.J. Crane, Flow past a stretching plate, Zeitschrift für angewandte Mathematik und Physik ZAMP 21 (1970) 645–647.
[21] L. Rani Titus, A. Abraham, Flow of Ferrofluid Over an Inclined Stretching Sheet in the Presence of a Magnetic Dipole, The World Congress on Engineering, Springer, 2019.
[22] A. Zeeshan, A. Majeed, Effect of magnetic dipole on radiative non-Darcian mixed convective flow over a stretching sheet in porous medium, Journal of Nanofluids 5 (4) (2016) 617–626.
[23] A. Zeeshan et al, Mixed convection flow and heat transfer in ferromagnetic fluid over a stretching sheet with partial slip effects, Therm. Sci. 22 (6 Part A) (2018) 2515–2526.
[24] R.P. Gowda et al, Exploring magnetic dipole contribution on ferromagnetic nanofluid flow over a stretching sheet: An application of Stefan blowing, J. Mol. Liq. 335 (2021) 116215.
[25] A. Hatamie et al, Evaluating magnetic nano-ferrofluid as a novel coagulant for surface water treatment, J. Mol. Liq. 219 (2016) 694–702.
[26] S.U. Choi, J.A. Eastman, *Enhancing thermal conductivity of fluids with nanoparticles*. 1995, Argonne National Lab.(ANL), Argonne, IL (United States).
[27] C. Scherer, A.M. Figueiredo Neto, Ferrofluids: properties and applications, Braz. J. Phys. 35 (2005) 718–727.
[28] N. Muhammad, S. Nadeem, Ferrite nanoparticles Ni-ZnFe2O4, Mn-ZnFe2O4 and Fe2O4 in the flow of ferromagnetic nanofluid, Europ. Phys. J. Plus 132 (9) (2017) 1–12.
[29] N. Muhammad, S. Nadeem, M. Mustafa, Analysis of ferrite nanoparticles in the flow of ferromagnetic nanofluid, PLoS One 13 (1) (2018) e0188460.
[30] S. Nadeem, S. Ahmad, N. Muhammad, Analysis of ferrite nanoparticles in liquid, Pramana 94 (1) (2020) 1–9.
[31] A. Majeed et al, Heat transfer in magnetite (Fe 3 O 4) nanoparticles suspended in conventional fluids: Refrigerant-134A (C 2 H 2 F 4), kerosene (C 10 H 22), and water (H 2 O) under the impact of dipole, Heat Transfer Research 51 (3) (2020).
[32] L. Ali et al, The impact of nanoparticles due to applied magnetic dipole in micropolar fluid flow using the finite element method, Symmetry 12 (4) (2020) 520.
[33] L. Ali et al, Analysis of magnetic properties of nano-particles due to a magnetic dipole in micropolar fluid flow over a stretching sheet, Coatings 10 (2) (2020) 170.
[34] M. Sheikholeslami, Magnetic source impact on nanofluid heat transfer using CVFEM, Neural Comput. Applic. 30 (4) (2018) 1055–1064.
[35] M. Sheikholeslami, New computational approach for exergy and entropy analysis of nanofluid under the impact of Lorentz force through a porous media, Comput. Methods Appl. Mech. Eng. 344 (2019) 319–333.

[36] H.V. Kiranakumar et al, A review on electrical and gas-sensing properties of reduced graphene oxide-metal oxide nanocomposites, Biomass Convers. Biorefin. (2022).
[37] R.N. Kumar et al, Impact of magnetic dipole on ferromagnetic hybrid nanofluid flow over a stretching cylinder, Phys. Scr. 96 (4) (2021) 045215.
[38] K. Anantha Kumar et al., *Effect of electromagnetic induction on the heat transmission in engine oil-based hybrid nano and ferrofluids: A nanotechnology application,* Proc. Inst. Mech. Eng., Part E: J. Process Mech. Eng. 2022, 09544089221139569.
[39] G. Ramesh et al, Thermodynamics examination of Fe 3 O 4-CoFe 2 O 4/water+ EG nanofluid in a heated plate: crosswise and stream-wise aspects, Arab. J. Sci. Eng. (2021) 1–10.
[40] S. Zainodin et al, Effects of higher order chemical reaction and slip conditions on mixed convection hybrid ferrofluid flow in a Darcy porous medium, Alex. Eng. J. 68 (2023) 111–126.
[41] S. Ullah et al, Optimal control analysis of tuberculosis (TB) with vaccination and treatment, Europ. Phys. J. Plus 135 (7) (2020) 602.
[42] M.A. Khan et al, Prevention of Leptospirosis Infected Vector and Human Population by Multiple Control Variables, Abstract Appl. Analy. 2014 (2014) 619035.
[43] A. Khan et al, Fractional dynamics and stability analysis of COVID-19 pandemic model under the harmonic mean type incidence rate, Comput. Methods Biomech. Biomed. Eng. 25 (6) (2022) 619–640.
[44] S. Nadeem, S. Ahmad, N. Muhammad, Analysis of ferrite nanoparticles in liquid, Pramana 94 (2020) 1–9.
[45] L. Rani Titus, A. Abraham, *Flow of Ferrofluid Over an Inclined Stretching Sheet in the Presence of a Magnetic Dipole*, in: *Transactions on Engineering Technologies: World Congress on Engineering 2018 26*. 2019. Springer.
[46] S.K. Das et al., *Nanofluids: science and technology*, John Wiley & Sons, 2007.
[47] H. Garg, A.S. Kharola, V. Karar, Numerical Analysis of Different Magnet Shapes on Heat Transfer Application using Ferrofluid, *Proceedings of the 2015 COMSOL Conference*, 2015.
[48] K.G. Kumar et al, A novel approach for investigation of heat transfer enhancement with ferromagnetic hybrid nanofluid by considering solar radiation, Microsyst. Technol. 27 (1) (2021) 97–104.
[49] M. Akbari et al, An experimental study on rheological behavior of ethylene glycol based nanofluid: proposing a new correlation as a function of silica concentration and temperature, J. Mol. Liq. 233 (2017) 352–357.
[50] T. Chen, A. Mucoglu, Analysis of mixed forced and free convection about a sphere, Int. J. Heat Mass Transf. 20 (8) (1977) 867–875.
[51] T. Cebeci, P. Bradshaw, *Physical and computational aspects of convective heat transfer*, Springer, New York, 1988.
[52] M. Malik et al, Variable viscosity and MHD flow in Casson fluid with Cattaneo-Christov heat flux model: Using Keller box method, Eng. Sci. Technol., Int. J. 19 (4) (2016) 1985–1992.
[53] F. Incropera et al., *Fundamentals of Heat and Mass Transfer 6th Edition, Fundamentals of Heat and Mass Transfer*, 2007.